Original Article

Inhibition of miR-9-3p facilitates ferroptosis by activating SAT1/p53 pathway in lung adenocarcinoma

Anqi Wu[1#], Anping Zhang[2#], Tianyi Wang[1], Jianle Chen[1,3,4], Jiahai Shi[1,3,4,5]

[1]Department of Thoracic Surgery, Affiliated Hospital of Nantong University, Medical School of Nantong University, Nantong, China; [2]Department of Cardiac Surgery, The Second Affiliated Hospital of Nantong University, Nantong, China; [3]Nantong Key Laboratory of Translational Medicine in Cardiothoracic Diseases, Affiliated Hospital of Nantong University, Nantong, China; [4]Research Institution of Translational Medicine in Cardiothoracic Diseases, Affiliated Hospital of Nantong University, Nantong, China; [5]School of Public Health, Nantong University, Nantong, China

Contributions: (I) Conception and design: A Wu, A Zhang; (II) Administrative support: J Chen, J Shi; (III) Provision of study materials or patients: T Wang; (IV) Collection and assembly of data: A Wu, A Zhang; (V) Data analysis and interpretation: A Wu, A Zhang, T Wang; (VI) Manuscript writing: All authors; (VII) Final approval of manuscript: All authors.

[#]These authors contributed equally to this work.

Correspondence to: Jianle Chen, MD. Department of Thoracic Surgery, Affiliated Hospital of Nantong University, Medical School of Nantong University, No. 20 Xisi Road, Nantong 226001, China; Nantong Key Laboratory of Translational Medicine in Cardiothoracic Diseases, Affiliated Hospital of Nantong University, Nantong 226001, China; Research Institution of Translational Medicine in Cardiothoracic Diseases, Affiliated Hospital of Nantong University, Nantong 226001, China. Email: Nanjingjn292@163.com; Jiahai Shi, MD. Department of Thoracic Surgery, Affiliated Hospital of Nantong University, Medical School of Nantong University, No. 20 Xisi Road, Nantong 226001, China; Nantong Key Laboratory of Translational Medicine in Cardiothoracic Diseases, Affiliated Hospital of Nantong University, Nantong 226001, China; Research Institution of Translational Medicine in Cardiothoracic Diseases, Affiliated Hospital of Nantong University, Nantong 226001, China; School of Public Health, Nantong University, Nantong 226019, China. Email: sjh@ntu.edu.cn.

Background: Lung adenocarcinoma (LUAD) is the most common subtype of non-small cell lung cancer (NSCLC) and accounts for about 40% of all lung cancer cases. This research aims to investigate the effects of miR-9-3p on ferroptosis in LUAD cells and to elucidate its regulatory mechanisms. Studies have shown that LUAD is related to ferroptosis, and specific microRNAs (miRNA) are also related to ferroptosis. However, further research is needed to elucidate the mechanisms by which miR-9-3p induces ferroptosis in LUAD.

Methods: Our study comprehensively analyzed multiple databases to investigate miR-9-3p expression in LUAD tissues. Quantitative polymerase chain reaction (qPCR) was utilized to detect miR-9-3p levels in LUAD cells and tissues, examining its prognostic significance. Reactive oxygen species (ROS) and superoxide dismutase (SOD) assays assessed the impact of miR-9-3p on lipid peroxidation in LUAD cells. Dual-luciferase reporter assays were conducted to evaluate the binding affinity between miR-9-3p and target genes, while Western blotting and immunofluorescence were used to examine the regulation of miR-9-3p on downstream signaling pathways.

Results: We observed that miR-9-3p was upregulated in LUAD cells by qPCR, and the ferroptosis of LUAD cells increased upon treatment with erastin following the transfection of miR-9-3p inhibitor. Cell Counting Kit-8 (CCK-8), ROS, and SOD activity assays confirmed that inhibiting miR-9-3p enhanced lipid peroxidation in LUAD cells, contributing to higher rates of ferroptosis. Subsequent dual-luciferase reporter assays validated spermidine/spermine N1-acetyltransferase 1 (SAT1) as a target gene of miR-9-3p. Further Western blot confirmed that miR-9-3p regulated the expression of SAT1 and p53 proteins in p53 wild-type (WT) LUAD cells. Rescue experiments demonstrated that SAT1 was necessary for miR-9-3p to promote cell proliferation and suppress ferroptosis in p53 WT LUAD cells. Additionally, the effect of miR-9-3p on ferroptosis in LUAD cells was regulated by p53 signaling pathway.

Conclusions: Overall, these findings demonstrate that miR-9-3p negatively regulates ferroptosis in LUAD cells through SAT1 and p53 signaling pathway, suggesting that miR-9-3p plays a crucial role in

LUAD pathogenesis and targeting this miRNA with an inhibitor exhibits promising potential for the treatment of LUAD.

Keywords: MiR-9-3p; spermidine/spermine N1-acetyltransferase 1 (SAT1); p53 signaling pathway; lung adenocarcinoma (LUAD); ferroptosis

Submitted Aug 27, 2024. Accepted for publication Nov 26, 2024. Published online Dec 27, 2024.
doi: 10.21037/tlcr-24-762
View this article at: https://dx.doi.org/10.21037/tlcr-24-762

Introduction

Lung cancer is characterized by high mortality rates (1), and can be classified into small cell lung cancer (SCLC) and non-SCLC (NSCLC) (2). Among the NSCLC histological types, lung adenocarcinoma (LUAD) is the most prevalent (3). Of note, the majority of patients with LUAD are diagnosed at advanced stages of the disease. Despite advancements in treatment, including immunotherapy, over recent decades, a significant proportion of patients with LUAD have shown limited response, and the prognosis of LUAD remains grim, with a 5-year survival of 8% (4-6). Thus, it is vital to identify new biological targets that can aid in the treatment of LUAD (7,8).

Highlight box

Key findings

- The increased expression of miR-9-3p in lung adenocarcinoma (LUAD) was associated with poor prognosis of LUAD. Moreover, miR-9-3p negatively regulated ferroptosis through spermidine/spermine N1-acetyltransferase 1 (SAT1) and p53 signaling pathways in LUAD cells.

What is known and what is new?

- Previous studies have highlighted the function of miR-9-3p in different cancer types. For example, miR-9-3p has been identified as a regulator of apoptosis and proliferative activity of glioma cells, while it has been reported to inhibit carcinogenic activity of liver cancer. However, no relationship between miR-9-3p and ferroptosis has been reported.
- In the present study, inhibition of miR-9-3p enhanced the susceptibility of LUAD cells to erastin-induced ferroptosis. Importantly, the study also revealed the critical role of p53 signaling in mediating the regulatory effect of miR-9-3p/SAT1 on ferroptosis in LUAD.

What is the implication, and what should change now?

- This study highlights the promise of targeting miR-9-3p as a new therapeutic approach for the treatment of LUAD, especially in combination with erastin to induce ferroptosis cell death. Further studies are needed to make miR-9-3p a therapeutic target for LUAD patients.

Several studies have demonstrated the link between LUAD and ferroptosis (9,10). Ferroptotic cell death, initially discovered in 2012, is functionally and morphologically different from necrosis or apoptosis (11). This iron-dependent process is characterized by elevated reactive oxygen species (ROS) and extensive lipid peroxidation within cells (12), resulting in alterations in mitochondrial function and morphology, as well as an increase in mitochondrial membrane density (13). In this context, Fe^{2+} within cells can catalyze the peroxidation of unsaturated fatty acids in the cell membrane, ultimately promoting cell death (14). Enhanced ferroptotic activity can be detected, in part, through key antioxidant factors like glutathione (GSH) and GSH peroxidase 4 (GPX4) (15,16). However, more research on LUAD and ferroptosis needs to be explored further.

MicroRNAs (miRNAs) are short, highly conserved noncoding transcripts consisting of approximately 22 nucleotides. They primarily affect cellular behaviors such as proliferation, autophagy, and survival by regulating specific target genes posttranscriptionally (17-19). Recent work has also linked specific miRNAs to ferroptotic activity (20,21). For example, miR-424-5p targets acyl-CoA synthetase long-chain family member 4 (ACSL4) to inhibit ferroptosis in ovarian cancer cells (22); miR-190a-5p controls cardiomyocyte ferroptosis (23); and miR-19a suppresses recombinant iron responsive element binding protein 2 (IREB2) expression to prevent ferroptosis induction in colorectal cancer cells (24). MiR-9-3p, a mature form of miR-9, has been extensively studied and has been found to be involved in tumor development across various cancer types (25,26). While many studies have explored the roles of miRNAs in LUAD (27-30), the specific connection between miR-9-3p and ferroptosis, as well as its role in LUAD, has not been documented thus far.

In this study, the impact of miR-9-3p on ferroptosis was

investigated in LUAD cells. To explore its role, LUAD cells were treated with a widely studied ferroptosis inducer, erastin (31,32). Additionally, the regulatory mechanism underlying miR-9-3p's involvement in ferroptotic cell in LUAD was examined by transfecting immortalized LUAD cells with either miR-9-3p mimic or inhibitor. We present this article in accordance with the ARRIVE and MDAR reporting checklists (available at https://tlcr.amegroups.com/article/view/10.21037/tlcr-24-762/rc).

Methods

Patient tissue specimens

Fresh tumor tissues and adjacent non-tumor tissues were obtained from the Affiliated Hospital of Nantong University. All patients included in the study were diagnosed with LUAD based on clinical and pathological assessments. Following excision, the tissues were promptly stored in liquid nitrogen and subsequently preserved in a freezer set at –80 ℃ for subsequent RNA or protein extraction. For human experiments, the study was conducted in accordance with the Declaration of Helsinki (as revised in 2013). The study was approved by the Ethics Committee of the Affiliated Hospital of Nantong University (ethical review report number: 2022-L165) and informed consent was obtained from all individual participants.

Cell culture and cell transfection

The human NCI-H1299, PC9, A549, NCI-H1975, HCC827, NCI-H23, and NCI-H1650 NSCLC cell lines (mycoplasma-free cells) were obtained from the National Collection of Authenticated Cell Cultures, Chinese Academy of Sciences (Shanghai, China). All cells were cultured in RPMI-1640 medium (Corning, Corning, NY, USA) containing 1% penicillin-streptomycin-amphotericin B (Beyotime, Shanghai, China) and 10% fetal bovine serum (FBS) in a 37 ℃, 5% CO_2 incubator. Lipofectamine 3000 (Invitrogen, Waltham, MA, USA) was used to transfect cells based on the provided instructions. For the relevant experiments, cells were treated with specific compounds, including erastin, ferrostatin-1, Z-VAD-FMK, or necrostatin-1 (MedChemExpress, Shanghai, China). The final concentration of miR-mimics and inhibitors is 50 nM. The sequences of the miR-9-3p mimic and inhibitor used in the study are provided as follows: miR-9-3p mimic negative control (NC) sequence: UUUGUACUACACAAAAGUACUG; miR-9-3p mimic sequence: AUAAAGCUAGAUAACCGAAAGU; miR-9-3p inhibitor NC sequence: CAGUACUUUUGUGUAGUACAAA; miR-9-3p inhibitor sequence: ACUUUCGGUUAUCUAGCUUUAU. The spermidine/spermine N1-acetyltransferase 1 (SAT1) knockdown plasmid sequence included the sh1-SAT1 sequence GAGGGTTGGAGACTGTTCA and the sh2-SAT1 sequence GCACATGCACTTCTTGGT. TP53 status of these cell lines was displayed in Table S1.

Quantitative polymerase chain reaction (qPCR)

TRIzol (Thermo Fisher Scientific, Waltham, MA, USA) was used to extract RNA from tissues or cells, followed by the preparation of cDNA with a PrimeScript RT kit (Thermo Fisher Scientific). The qPCR analyses were conducted on a Roche Lightcycler 480 (Roche, Basel, Switzerland) with the following thermocycler settings: 95 ℃ for 10 min; 45 cycles of 90 ℃ for 15 s, 42 ℃ for 30 s, and 70 ℃ for 30 s. A melt curve analysis was then conducted to confirm the specificity of the amplification. Relative expression was assessed using the $2^{-\Delta\Delta Ct}$ method, and 18S served as a normalization control. The primers for qPCR used were listed below: SAT1 forward, 5'-ACCCGTGGATTGGCAAGTTAT-3'; SAT1 reverse, 5'-TGCAACCTGGCTTAGATTCTTC-3'; 18S forward, 5'-CGGCTACCACATCCAAGGAA-3'; 18S reverse, 5'-GCTGGAATTACCGCGGCT-3'.

Luciferase reporter assays

Cells in 24-well plates were co-transfected with miR-9-3p mimic and wild-type (WT) SAT1 or mutant SAT1 reporter plasmids using Lipofectamine 3000 (Invitrogen). At 48 hours after transfection, luciferase activity in the cell lysates was measured using a dual luciferase kit (Vazyme, Nanjing, China). The experiments were repeated in triplicate.

Viability assay

A Cell Counting Kit-8 (CCK-8; MedChemExpress) was utilized according to the manufacturer's instructions. After plating cells in 96-well plates (3,000/well) for 24 hours, medium supplemented with 10 μL of CCK-8 reagent was added to each well. The plates were further incubated for 2 hours at 37 ℃, and then the absorbance was measured at 450 nm.

5-ethynyl-2'-deoxyuridine (EdU) uptake assay

Cell proliferation was assessed with a EdU kit (RiboBio, Guangzhou, China). After transfection, cells were added to 24-well plates (3×10^4/well) and incubated for 24 hours, followed by the addition of EdU solution (50 mM) to each well. Following a 2-hour incubation, the cells were fixed with precooled 4% paraformaldehyde for half an hour. After 5 min of decolorization with glycine, the cells were washed with phosphate-buffered saline (PBS). Cells were incubated in a shaker with penetrant (PBS of TritonX-100) for 10 min. The cells were stained with Apollo and Hoechst 33342 solution, and a fluorescence microscope was used to assess the rate of cell EdU positivity.

Transwell assays

For migration and invasion assays, 7×10^4 and 5×10^4 cells in 500 µL of serum-free medium were added to the upper chamber of uncoated and Matrigel-coated Transwell inserts, respectively, with 600 µL of RPMI-1640 supplemented with 20% FBS added to the lower chamber in both cases. After incubation for 24–48 hours incubation, cells in the upper chamber were brushed away using a cotton swab, while those in the lower chamber were fixed for 30 min using 4% paraformaldehyde, stained for 15 min with crystal violet, and subsequently counted under a microscope.

Colony formation assays

After plating in 6-well plates (1,000/well) and incubation for 2 weeks, cells were subjected to fixation for 30 min using 4% paraformaldehyde (Biosharp, Shanghai, China), and staining for 15 min with 0.1% crystal violet (Biosharp). Then the visible colonies were counted.

Western blotting

Lysis buffer containing phenylmethylsulfonyl fluoride (PMSF; SolarBio, Beijing, China) was used to extract proteins from samples, and a bicinchoninic acid (BCA) protein detection kit (P0009, Beyotime) was used to calculate protein concentrations prior to protein separation via sodium dodecyl sulfate-polyacrylamide gel electrophoresis (SDS-PAGE). The proteins were then transferred to polyvinylidene fluoride (PVDF) membranes, and blots were blocked for a 2-hour interval using 5% skim milk at room temperature, incubated overnight with primary antibodies (1:1,000) at 4 ℃, and probed at room temperature for 2 hours with secondary anti-rabbit immunoglobulin G (IgG; 1:10,000; Proteintech, Wuhan, China) after three washes with Tris-buffered saline with Tween 20 (TBST). After being washed more than three times, the protein bands were detected with a high-sensitivity enhanced chemiluminescence (ECL) kit (Vazyme), and ImageJ was used for densitometric analyses. Primary antibodies targeting the following proteins were used: SAT1 (1:1,000; Proteintech), p53 (1:1,000; Proteintech), solute carrier family 7 member 11 (SLC7A11; 1:1,000; Proteintech), and glyceraldehyde 3-phosphate dehydrogenase (GAPDH; 1:1,000; Proteintech).

Intracellular ROS analyses

ROS levels in cells were measured with 2,7-dichlorofluorescein diacetate (DCFH-DA; Beyotime) based on the provided instructions. Initially, cells in 6-well plates were rinsed with PBS, and then, 1 µL of DCFH-DA was combined with 1 mL of serum-free medium in each well, followed by a 30 min incubation at 37 ℃ under protection from light. Following three consecutive washes with PBS, the cells were subjected to flow cytometry analysis.

Measurement of malondialdehyde (MDA) levels

An MDA kit (Beyotime) was employed to assess the extent of lipid peroxidation within cells and measure ferroptotic cell death. Samples were combined with an MDA detection working solution based on the provided instructions, followed by boiling for 15 min at 100 ℃. After subsequent centrifugation at room temperature, the absorbance of the samples was assessed at 532 nm.

Intracellular reduced GSH/oxidized GSH (GSH/GSSG) content measurements

Reduced and GSSG levels in treated cells were measured with a commercial kit (Beyotime) based on the provided instructions. Briefly, cells were collected in a detection buffer, frozen in liquid nitrogen, thawed three times, and centrifuged for 10 min, the supernatants were collected for analysis. GSH/GSSG reagent was then added to the supernatants, mixed and rested for 2 min at room temperature. The absorbance at 412 nm was then assessed, with blank and positive control samples being analyzed in parallel. GSH/GSGG content levels were quantified using

an appropriate formula.

Superoxide dismutase (SOD) activity analysis

Cellular SOD activity was used as a gauge for intracellular ferroptosis and was measured with an SOD kit (Beyotime). Initially, cells were lysed, and the lysates were centrifuged to collect supernatants for analysis based on recommendation by the provider. Then, a WST-8/enzyme working solution and a reaction working solution were added and further incubated with samples at 37 ℃ for 30 min. Absorbance at 450 nm was then quantified, and SOD activity in individual samples was quantified according to instructions.

In vivo experiments

For animal experiments, experiments were performed under a project license (Tab of Animal Experimental Ethical Inspection number: S20230420-005) granted by the Laboratory Animal Center of Nantong University, in compliance with the national or institutional guidelines for the care and use of animals. A protocol was prepared before the study without registration. Twelve female 5-week-old nude mice weighing about 12 g were purchased from the Animal Research Center of Nantong University School of Medicine and randomized into four treatment groups, with three mice in each group. These four groups were treated with the following interventions: NC antagomir, miR-9-3p antagomir, a combination of NC antagomir and erastin, and a combination of miR-9-3p antagomir and erastin. All mice were subcutaneously implanted with 1×10^7 LUAD cells. When tumors were ~60 mm^3 in size, the animals were injected with either a miR-9-3p antagomir plasmid, a NC antagomir plasmid, or a combination of either of these two plasmids together with erastin (15 mg/kg). The tumor volume was monitored with a caliper while injections were given every other day for 30 days, and the injection concentration was 2 nmol per animal. Finally, the mice were euthanized, and tumors were harvested, weighed, and fixed with 4% paraformaldehyde after 30 days.

Immunohistochemical (IHC) and histological staining

After paraformaldehyde fixation, the tumors from mice were embedded in paraffin, sections were produced, and stained by hematoxylin-eosin (HE) for histological examination. IHC staining was performed with antibodies for Ki67 (1:400; Proteintech) and SAT1 (1:100; Proteintech) and incubation overnight, followed by secondary horseradish peroxidase (HRP)-conjugated anti-rabbit IgG (1:500; Proteintech) for 1 h. Diaminobenzidine was used for visualization, after which the slides were examined via microscopy.

Statistical analysis

Experiments were repeated three times, and the results were reported as the means ± standard deviations. GraphPad Prism v7.0 was used to analyze the data, with $P<0.05$ as the significance threshold. *, $P<0.05$; **, $P<0.01$; and ***, $P<0.001$.

Results

Erastin promotes the ferroptotic death of LUAD cells

Initially, the impact of erastin on the survival of H1299 and A549 cells was assessed using CCK-8 assays, which revealed a significant decrease in the viability of LUAD cell lines. Remarkably, treatment with the ferroptosis inhibitor, ferrostatin-1, was able to inhibit erastin-induced lethality, which was unaffected by the apoptosis inhibitor, Z-VAD-FMK, and necrosis inhibitor, necrosulfanilamide (Figure S1A). Analysis of ROS and MDA levels revealed an increase in both lipid peroxidation-related factors rose after erastin treatment in these cell lines, whereas ferrostatin-1 reversed this effect (Figure S1B-S1D). These findings confirmed the sensitivity of LUAD cells to erastin-induced ferroptosis.

LUAD cells exhibit upregulation of miR-9-3p, and inhibiting miR-9-3p attenuates the proliferation of erastin-treated LUAD cells

To find a miRNA that can serve as a good biomarker for LUAD, we selected miRNAs with significantly increased expression levels for further study because their $\log_2$fold changes were more than 2 and the P values were less than 0.05, as shown in the sequencing results (Figure S2A,S2B). An initial screening of the TCGA database revealed elevated expression levels of miR-9-3p in lung cancer patient tissue samples (Figure S2C). Therefore, miR-9-3p was chosen for further research. Subsequent qPCR analyses validated these findings by demonstrating significantly increased expression of this miRNA in 60 LUAD tumors compared to healthy control tissues (Figure S3A). Based on the analysis of pathological information of patients, the expression value of miR-9-3p was correlated with tumor size ($P=0.002$; Table S2). Moreover, the expression of miR-9-3p was

evaluated via qPCR in various cell types including BEAS-2B, H1650, H1975, A549, H23, PC9, HCC827, and H1299. The results revealed higher expression of miR-9-3p in LUAD cells compared to BEAS2B cells used as the control group (Figure S3B). We selected two cell lines (A549 and H23) with low expression levels for overexpression and two (H1299549 and H1975) with high expression levels for knockdown (Figure S3C). qPCR results confirmed that A549 transfected with miR-9-3p mimic and H1299 transfected with miR-9-3p inhibitor had greater statistical significance in miR-9-3p expression (Figure S3C). Therefore, A549 and H1299 cells were chosen for further analysis. Subsequently, cells were simultaneously treated with these constructs and erastin. CCK-8 assays revealed that the inhibition of miR-9-3p resulted in impaired LUAD cell survival and enhanced cell death upon erastin treatment (Figure S3D). Similarly, EdU uptake assays validated the ability of miR-9-3p inhibition to suppress the proliferation of erastin-treated LUAD cells (Figure S3E,S3F).

The inhibition of miR-9-3p facilitates robust ferroptotic death in erastin-treated LUAD cells

Then, A549 and H1299 cells were transfected with miR-9-3p mimic or inhibitor or corresponding NCs, followed by treatment with erastin for 24 h. When the cells were assessed via transmission electron microscopy, control cells exhibited morphologically normal mitochondria with intact cristae. In contrast, the mitochondria of miR-9-3p inhibitor-transfected cells were shrunken, with visible damage to the cristae (*Figure 1A*). MiR-9-3p mimic and inhibitor resulted in reductions and increases, respectively, in intracellular levels of the lipid peroxidation marker MDA following erastin treatment in these cells (*Figure 1B*). To further investigate these results, DCFH-DA was employed to quantify ROS levels in these LUAD cells. The results revealed that miR-9-3p mimic group suppressed the ROS levels, while miR-9-3p inhibitor enhanced the ROS levels in both H1299 and A549 cells following erastin treatment (*Figure 1C,1D*). Consistently, transfection of these LUAD cells with miR-9-3p mimic or inhibitor resulted in increased and decreased SOD activity, respectively (*Figure 1E*). The overexpression of miR-9-3p also led to increased intracellular GSH levels and reduced intracellular GSSG levels, which are negatively and positively correlated with ferroptosis, respectively, in these cells. This resulted in a net increase in the GSH/GSSG ratio. In contrast, the GSH/GSSG ratio declined when miR-9-3p was inhibited (*Figure 1F*). Thus, treatment with miR-9-3p inhibitor can enhance erastin-induced ferroptosis in LUAD cells, whereas transfection with miR-9-3p mimic can protect these cancer cells from ferroptotic death upon erastin treatment.

MiR-9-3p binds SAT1 to regulate p53

Next, candidate miR-9-3p target genes were analyzed using online databases, and six genes were identified through the cross-referencing of these targets with genes known to be associated with the ferroptosis pathway (*Figure 2A*). In the analysis of correlations between these identified 6 genes and the expression of miR-9-3p in LUAD tumor tissue samples, SAT1 expression exhibited the most striking inverse relationship with miR-9-3p levels (Figure S4A). A study has revealed that the activation of SAT1 promotes lipid peroxidation, thereby facilitating ferroptotic activity by inducing ROS-related damage (33). Additionally, SAT1 is regulated by the master tumor suppressor p53, which can control ferroptotic activity at the transcriptional and posttranslational levels. Accordingly, SAT1 was selected as a target gene for further validation. Subsequent qPCR analyses revealed that the overexpression of miR-9-3p resulted in a significant downregulation of SAT1 expression, whereas the inhibition of miR-9-3p had the opposite effect (*Figure 2B*). Further luciferase reporter assays confirmed that the activity of a WT SAT1 3'-untranslated region (3'-UTR) reporter construct was enhanced by transfection with miR-9-3p mimic, but not with mimic NC. Conversely, the activity of the mutant SAT1 3'-UTR reporter remained unaltered in both cases (*Figure 2C*). These data showed that miR-9-3p directly targets SAT1. A previous report has indicated that SAT1 promotes ferroptosis as a novel molecular mechanism in LUAD (34). However, it remains unclear whether this mechanism is associated with the upregulation of miR-9-3p. To validate this, 40 tumor and para-cancerous tissue samples from LUAD patients were collected. Consistently, qPCR analysis confirmed significantly reduced expression of SAT1 in cancer tissues compared to normal tissues ($P<0.01$). Similarly, Western blotting showed that SAT1 protein level in 14 tumor tissue samples were lower than that in paired para-cancerous normal tissues. The expression of SAT1 was also found to be low in LUAD cells (*Figure 2D,2E*), and qPCR analyses confirmed an inverse relationship between the expression of miR-9-3p and SAT1 in LUAD tissue samples (*Figure 2F*). Furthermore, LUAD cells were transfected with SAT1-specific short hairpin RNAs (shRNAs; sh1-SAT1 or

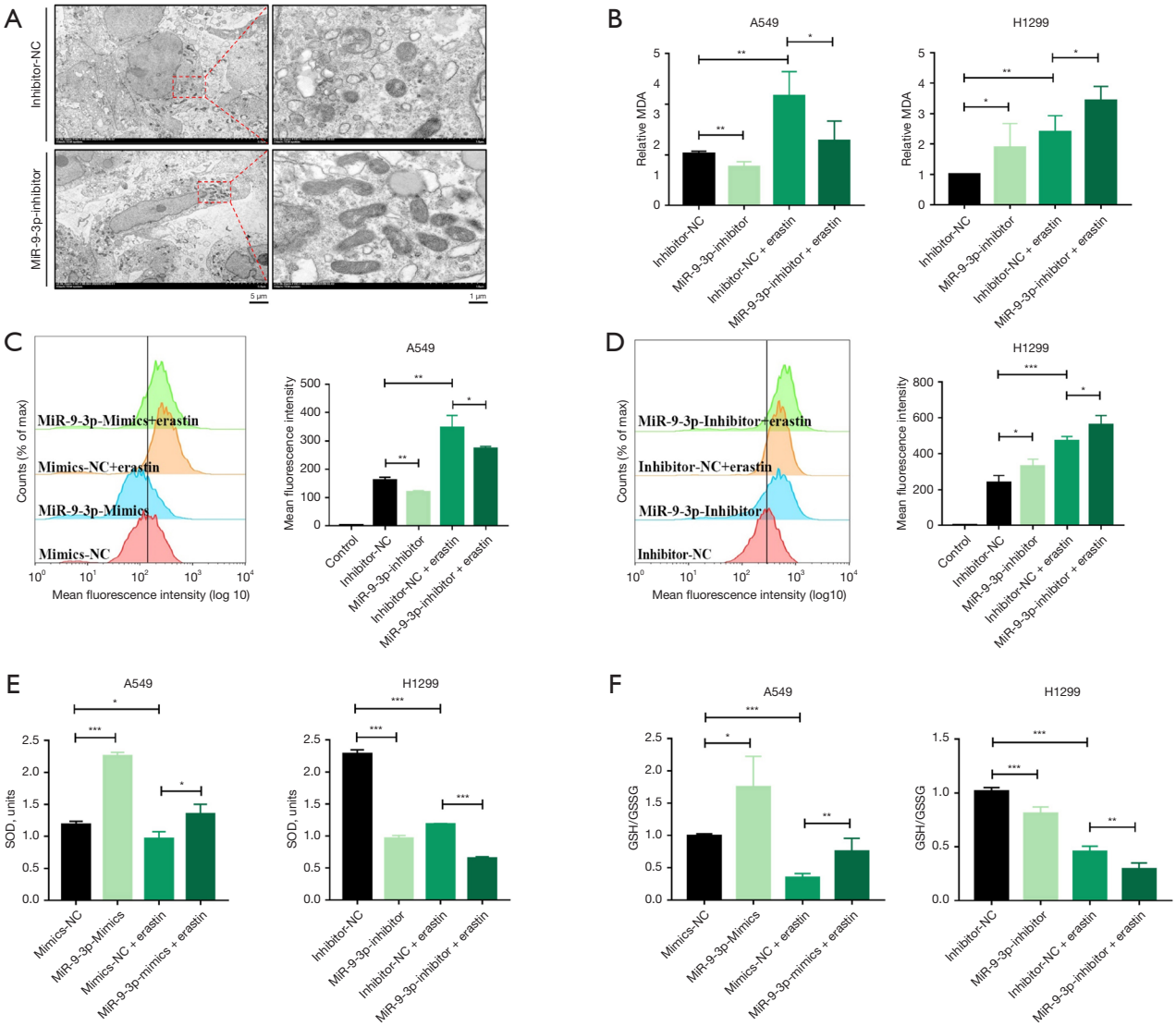

Figure 1 The impact of miR-9-3p on erastin-induced ferroptotic LUAD cell death. (A) The morphology of LUAD cell mitochondria was assessed via TEM. (B) The impact of miR-9-3p on MDA content within LUAD cells following erastin treatment was assessed with a commercial kit. (C,D) Flow cytometry was employed to gauge the impact of miR-9-3p on ROS levels within erastin-treated LUAD cells. (E) SOD activity in the indicated LUAD cells was measured with an appropriate kit. (F) GSH and GSSG levels were analyzed in LUAD cells using a commercial kit. *, P<0.05; **, P<0.01; ***, P<0.001 *vs.* corresponding NC group. Data are representative findings for three independent experimental replicates and are given as the mean ± SD. NC, negative control; MDA, malondialdehyde; LUAD, lung adenocarcinoma; TEM, transmission electron microscopy; ROS, reactive oxygen species; SOD, superoxide dismutase; GSH, glutathione; GSSG, oxidized glutathione; SD, standard deviation.

sh2-SAT1), miR-9-3p inhibitor, miR-9-3p mimic and a SAT1 overexpression construct. qPCR and western blot were used to validate the function of these knockdown and overexpression constructs in H1299 and A549 cells respectively (Figure S4B-S4F).

To further investigate the impact of miR-9-3p on p53 and SAT1 protein expression, Western blotting was conducted. The results revealed that in p53 WT LUAD cells, transfection with miR-9-3p mimic led to a decrease in the expression of both p53 and SAT1 proteins, while transfection with miR-9-3p inhibitor resulted in an increase in the expression of both proteins

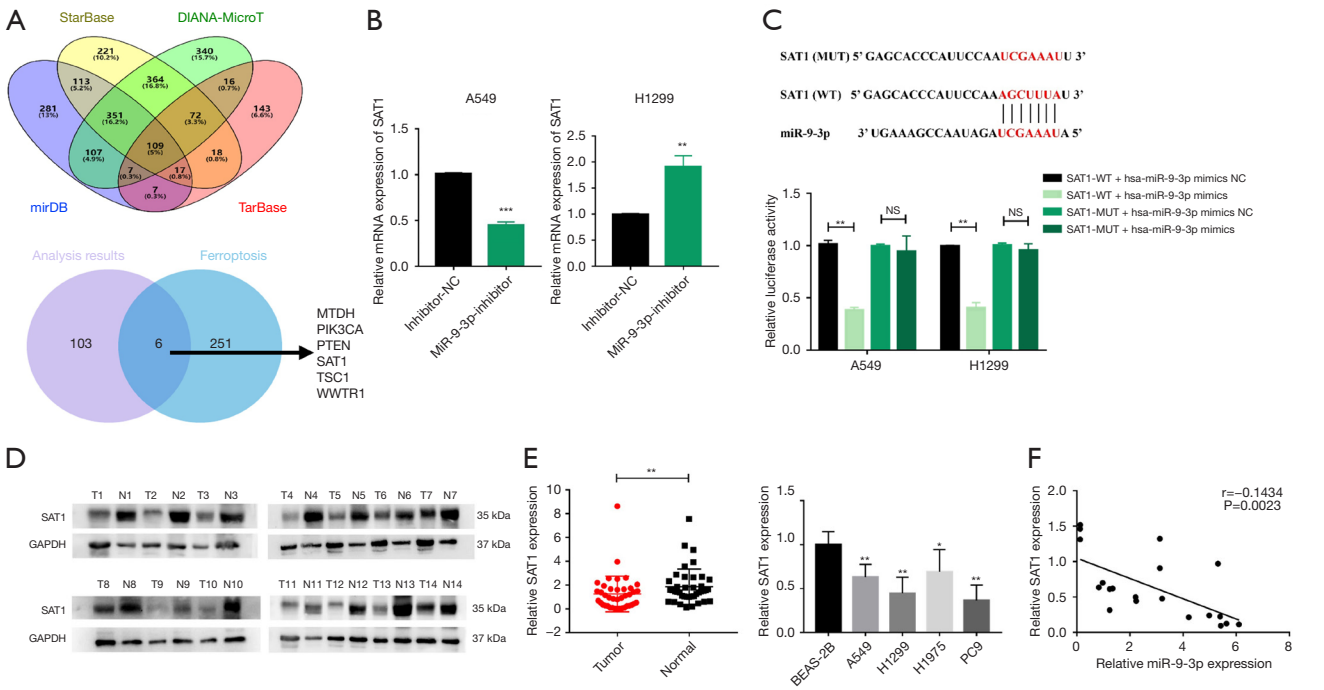

Figure 2 SAT1 is a direct miR-9-3p target. (A) A Venn diagram highlighting the overlap between miR-9-3p targets predicted by various databases. (B) SAT1 levels following miR-9-3p overexpression or silencing were assessed via qRT-PCR. (C) Cells were cotransfected with miR-9-3p mimic and WT or mutant SAT1 3'-UTR reporter plasmids, and luciferase activity was measured using a dual-luciferase reporter assay. (D,E) SAT1 levels were analyzed in LUAD tissue and cell samples via Western blotting and qPCR. (F) A negative correlation between miR-9-3p and SAT1 expression was observed in samples of LUAD patient tumor tissues. P=0.002. *, P<0.05; **, P<0.01; ***, P<0.001 *vs.* corresponding NC group. Data are representative findings for three independent experimental replicates and are given as the mean ± SD. mRNA, messenger RNA; SAT1, spermidine/spermine N1-acetyltransferase 1; NC, negative control; WT, wild-type; MUT, mutant; NS, not significant; GAPDH, glyceraldehyde 3-phosphate dehydrogenase; T, tumor; N, normal; qRT-PCR, quantitative real-time PCR; PCR, polymerase chain reaction; 3'-UTR, 3'-untranslated region; qPCR, quantitative PCR; LUAD, lung adenocarcinoma; SD, standard deviation.

(Figure S5A,S5B). These findings were further confirmed through cell immunofluorescence experiments, which also demonstrated a consistent decrease in p53 and SAT1 protein expression upon miR-9-3p mimic transfection, and an increase upon miR-9-3p inhibitor transfection (Figure S5C-S5F). However, miR-9-3p had no significant effect on p53 and SAT1 protein expression levels in p53 mutant LUAD cells (Figure S6A). To further verify the interaction between miR-9-3p and SAT1, we co-transfected miR-9-3p-mimics or miR-9-3p-inhibitor and SAT1 plasmids into A549 and H1299 cells. It was observed that SAT1 overexpression and knockdown were able to reverse the inhibitory and promoting effects, respectively, on the SAT1 and p53 pathways, suggesting that miR-9-3p may regulate ferroptotic activity through targeting these pathways (Figure S6B-S6E). In summary, miR-9-3p binds to SAT1 to regulate p53 expression and promote tumor growth in p53 WT LUAD cells.

Overexpression of miR-9-3p reverses the inhibitory impact of SAT1 on proliferation, migration and invasive in p53 WT LUAD cells

In CCK-8 assays, overexpression of SAT1 resulted in a significant reduction in the viability of LUAD cells, whereas the transfection of miR-9-3p mimic led to a significant enhancement of cell viability in the context of SAT1 overexpression. Similarly, knockdown of SAT1 improved LUAD cell viability, whereas the inhibition of miR-9-3p in the context of SAT1 silencing caused a decreased in cell viability (*Figure 3A,3B*). EdU uptake and colony formation assays confirmed the ability of miR-9-3p mimic to reverse the inhibitory effect on LUAD cell proliferation caused by SAT1 overexpression, while inhibition of

miR-9-3p reversed the enhanced proliferation observed with SAT1 knockdown in LUAD cells (*Figure 3C-3F*). Transwell assays also demonstrated that overexpression of SAT1 resulted in a notable inhibition of LUAD cell migration and invasion However, when miR-9-3p mimic was transfected, this effect was reversed. Conversely, when SAT1 was silenced, LUAD cell migration and invasion were significantly enhanced. Interestingly, this effect was reversed following co-transfection with miR-9-3p inhibitor (*Figure 3G,3H*).

Overexpression of miR-9-3p reverses the ability of SAT1 to promote lipid peroxidation and ferroptosis in p53 WT LUAD cells

Using a flow cytometry-based approach, the overexpression of SAT1 was found to enhance ROS accumulation within LUAD cells, whereas transfection with miR-9-3p mimic reversed this effect. In contrast, the knockdown of SAT1 decreased the ROS levels in these cancer cells, while transfection of miR-9-3p inhibitor led to an increase in ROS levels in the context of SAT1 knockdown (*Figure 4A,4B*). An MDA kit was further employed to detect the levels of this byproduct of lipid peroxidation. The results revealed that transfection of cells with a miR-9-3p mimic reversed the ability of SAT1 overexpression to enhance MDA levels. Conversely, inhibition of miR-9-3p reversed the reduction in MDA levels observed in cells with SAT1 knockdown (*Figure 4C*). Consistent with these results, measurements of the key antioxidant enzyme SOD revealed that transfection with miR-9-3p mimic rescued SAT1 overexpression-induced decreases in SOD activity, while the inhibition of miR-9-3p reversed the increased SOD activity (*Figure 4D*). In addition, transmission electron microscopy observed that compared with the control group, LUAD cells in the SAT1 knockdown group exhibited normal mitochondrial morphology with intact and uniform mitochondrial cristae. However, after co-transfection of miR-9-3p mimics, mitochondrial shrinkage and damage to the mitochondrial cristae were observed in LUAD cells (*Figure 4E*).

MiR-9-3p regulates ferroptosis through p53 signaling pathway

To verify whether miR-9-3p affects ferroptosis through the p53 signaling pathway, we performed rescue experiments using the p53 pathway inhibitor pifithrin-α. ROS assay was used to detect the content of ROS in LUAD cells. The results showed that pifithrin-α could restore the effect of miR-9-3p inhibitor on ferroptosis (*Figure 5A*). In addition, the results of CCK-8 experiments revealed that pifithrin-α can rescue the effect of miR-9-3p inhibitor on cell viability (*Figure 5B*). After LUAD cells transfected with inhibitor-NC or miR-9-3p-Inhibitor were treated with or without pifithrin-α, the expression levels of p53 and SLC7A11 expression were detected by Western blotting (*Figure 5C-5E*). These results suggest that the p53 signaling pathway is necessary for miR-9-3p-mediated ferroptosis.

Inhibiting miR-9-3p enhances erastin-induced ferroptotic death in xenograft tumors in vivo

To further validate the inhibitory role of miR-9-3p in erastin-driven ferroptotic LUAD cell death *in vivo*, a murine xenograft model system was established. Nude mice were subcutaneously implanted with 1×10^7 LUAD cells. After 1 week, when tumors were visible, the animals were separated into four groups that were treated with antagomir-9-3p or a corresponding control with or without erastin (*Figure 6A*). Following treatment for 1 month, it was observed that the tumor growth rate was significantly slower in the antagomir-9-3p treatment group compared to control group. Furthermore, the tumor growth rate was even further reduced in the group treated with antagomir-9-3p and erastin (*Figure 6B,6C*). Both qPCR and Western blotting analyses revealed that inhibition of miR-9-3p led to an upregulation of SAT1 expression these xenograft tumors (*Figure 6D*). HE and IHC staining demonstrated a reduce in tumor cell proliferation upon antagomir-9-3p treatment, which was further decreased under the combination of antagomir-9-3p and erastin. Moreover, the expression levels of SAT1 rose in the antagomir-9-3p group compared to the control group, and these levels were even higher in the combination group. Together, these findings suggest that the combination of miR-9-3p inhibition and erastin treatment can effectively interfere with LUAD tumor growth *in vivo* (*Figure 6E*).

Discussion

The three biochemical processes involved in ferroptosis are iron metabolism, amino acid and GSH metabolism, and lipid metabolism. This research elaborates on the changes in ROS levels during the occurrence of ferroptosis, as well as the main regulatory mechanisms of GSH metabolism and

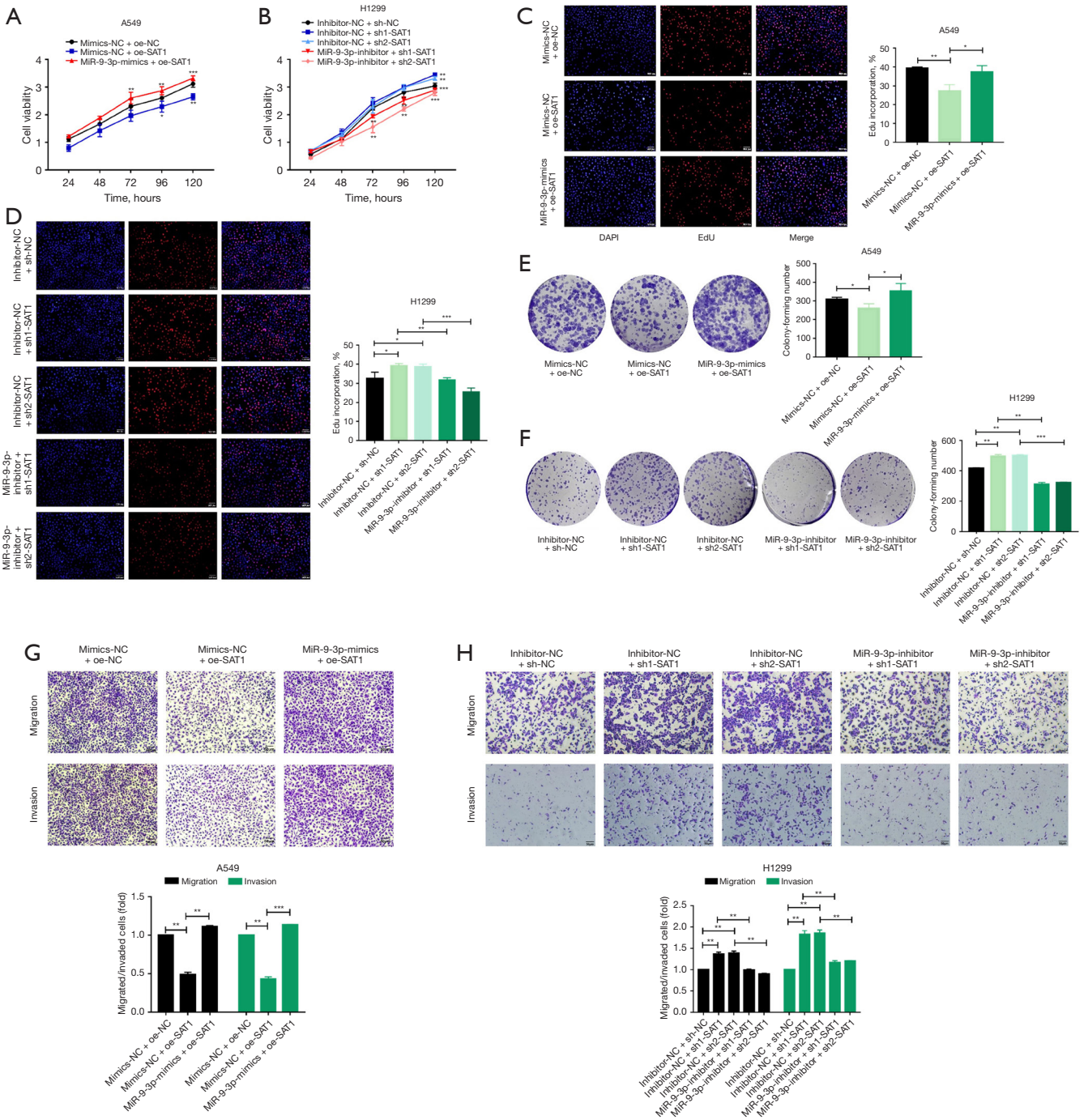

Figure 3 The miR-9-3p-mediated suppression of SAT1 expression influences p53 WT LUAD cell proliferation, migration, and invasion activities. (A,B) LUAD cell viability was assessed via CCK-8 assays. (C-F) The impact of miR-9-3p-mediated SAT1 targeting on LUAD cell proliferation was examined through EdU uptake and colony formation assays. For EdU staining, the cells were stained with apollo and the nucleus was labeled with DAPI. Scale bar, 100 μm. The staining method of colony assay was crystal violet staining. Scale bar, 100 μm. (G,H) Transwell assays were used to examine the effects of miR-9-3p-mediated SAT1 targeting on LUAD cell migration and invasion activities. The staining method was crystal violet staining. Scale bar, 100 μm. *, P<0.05; **, P<0.01; ***, P<0.001 *vs.* corresponding NC group. Data are representative findings for three independent experimental replicates and are given as the mean ± SD. NC, negative control; oe, overexpression; SAT1, spermidine/spermine N1-acetyltransferase 1; sh, short hairpin; DAPI, 4',6-diamidino-2-phenylindole; EdU, 5-ethynyl-2'-deoxyuridine; WT, wild-type; LUAD, lung adenocarcinoma; CCK-8, Cell Counting Kit-8; SD, standard deviation.

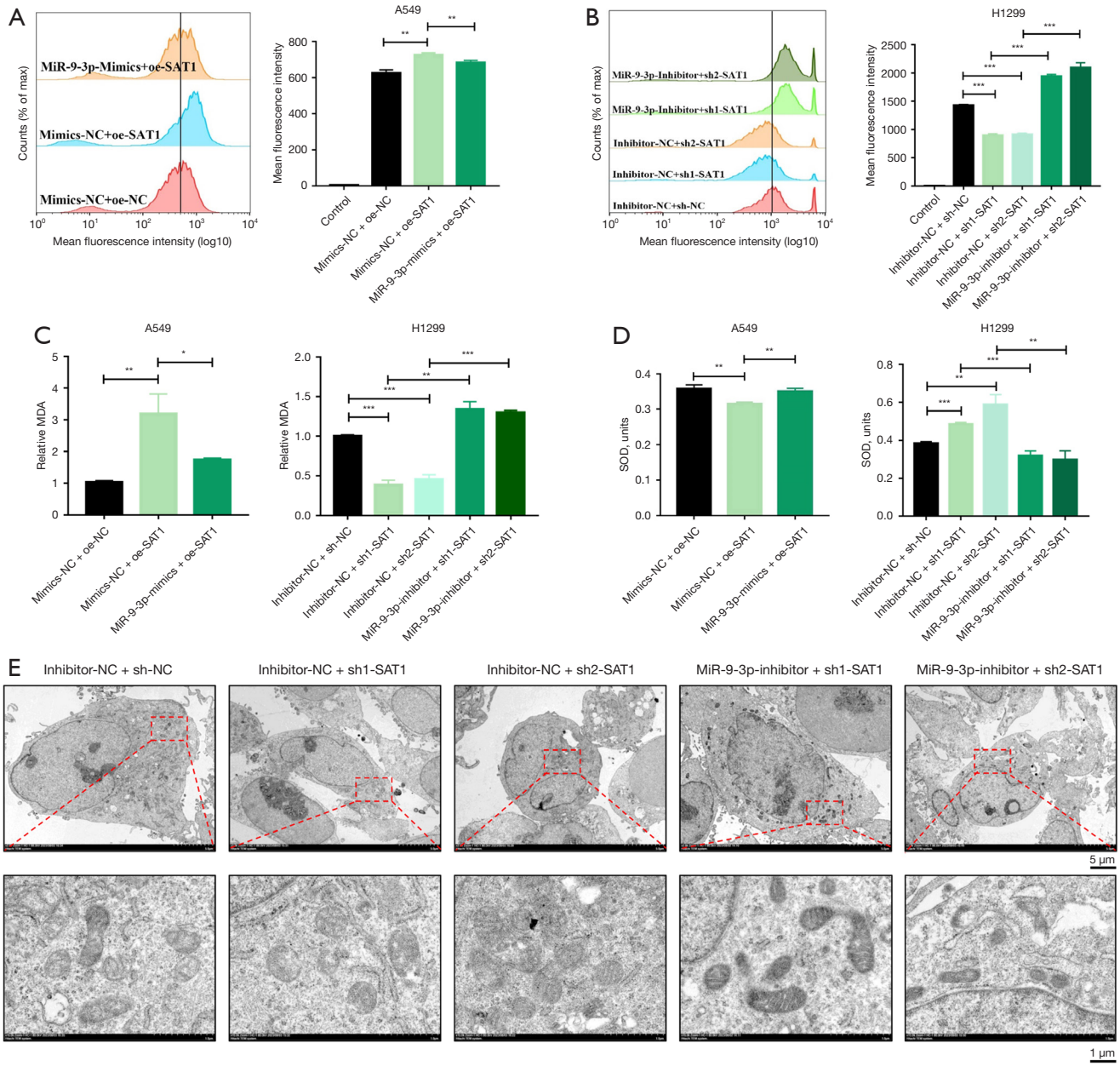

Figure 4 The miR-9-3p-mediated regulation of SAT1 expression influences ferroptotic cell death in p53 WT LUAD cells. (A,B) ROS levels were analyzed via flow cytometry. (C) MDA levels were assessed to gauge lipid peroxide levels in LUAD cells in the context of the miR-9-3p-mediated targeting of SAT1. (D) SOD activity levels were assessed with a commercial kit. (E) TEM was used to observe the morphology of mitochondria in LUAD cells with the miR-9-3p-mediated targeting of SAT1. *, P<0.05; **, P<0.01; ***, P<0.001 *vs.* corresponding NC group. Data are representative findings for three independent experimental replicates and are given as the mean ± SD. oe, overexpression; NC, negative control; SAT1, spermidine/spermine N1-acetyltransferase 1; sh, short hairpin; MDA, malondialdehyde; SOD, superoxide dismutase; WT, wild-type; LUAD, lung adenocarcinoma; ROS, reactive oxygen species; TEM, transmission electron microscopy; SD, standard deviation.

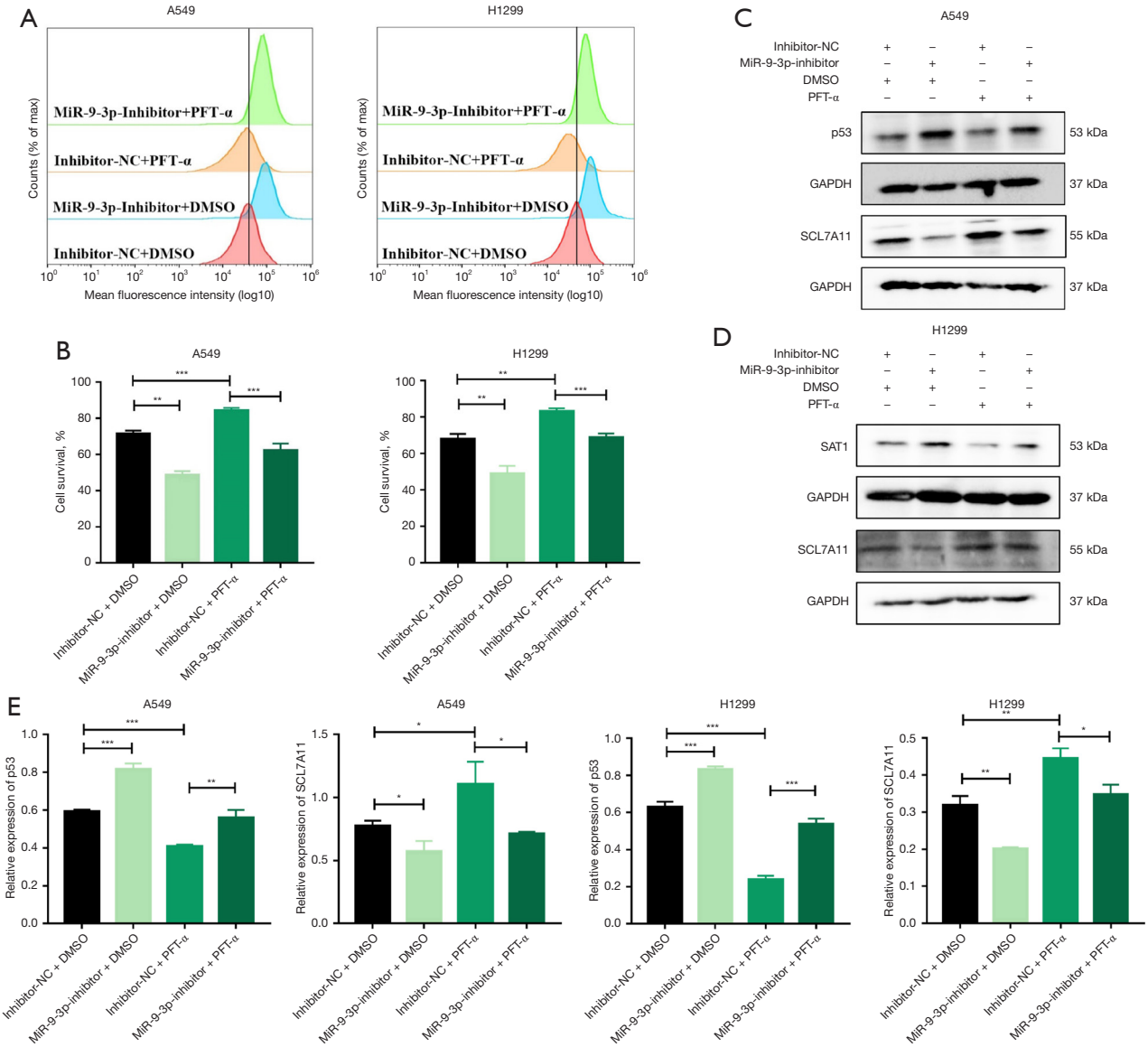

Figure 5 P53 signaling pathway mediates miR-9-3p to regulate ferroptosis. (A) ROS levels were detected by flow cytometry. (B) Cell viability was detected by CCK-8 assay. (C-E) The expression of p53 and SLC7A11 was detected by Western blot. *, P<0.05; **, P<0.01, ***, P<0.001 *vs*. corresponding NC group. Data are representative findings for three independent experimental replicates and are given as the mean ± SD. NC, negative control; DMSO, dimethyl sulfoxide; GAPDH, glyceraldehyde 3-phosphate dehydrogenase; SLC7A11, solute carrier family 7 member 11; ROS, reactive oxygen species; CCK-8, Cell Counting Kit-8; SD, standard deviation.

their roles in the development and progression of LUAD. Specifically, we found that inhibition of miR-9-3p enhances the susceptibility of LUAD cells to erastin-induced ferroptosis. Importantly, the investigation also unveiled the crucial involvement of the p53 signaling pathway in mediating the regulatory effects of miR-9-3p/SAT1 on ferroptosis in LUAD, providing valuable insights into the pathogenesis of LUAD (Figure S7).

Several milestones have been achieved in identifying driver mutations that allow the use of targeted inhibitors for LUAD (35). Furthermore, our current knowledge of lung cancer has been significantly enhanced through advancements in immunotherapy and the exploration of the tumor microenvironment (TME). However, the pathogenic,

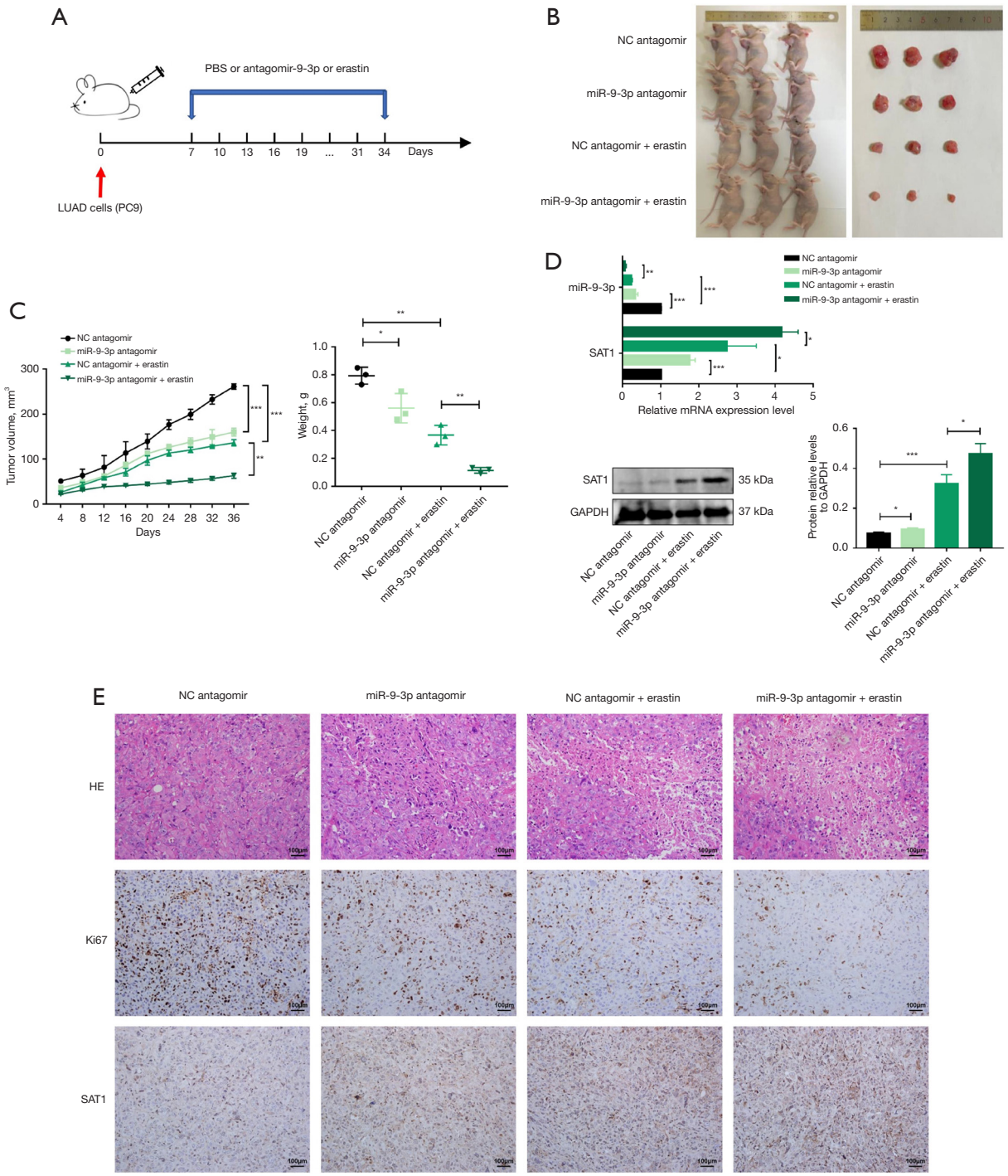

Figure 6 Inhibiting miR-9-3p enhances ferroptotic activity in xenograft LUAD tumors *in vivo*. (A) Schematic overview of the tumor implantation and treatment approach for this experiment using nude mice. (B) Tumor growth was inhibited by miR-9-3p inhibitor and erastin treatment. (C) Tumor volume and weight measurements. (D) Western blotting was used to assess miR-9-3p and SAT1 expression in xenograft tumors. (E) HE staining was used to detect necrosis in tumor tissues, while Ki67 and SAT1 expression levels were analyzed via IHC. *, P<0.05; **, P<0.01; ***, P<0.001 *vs*. corresponding NC group. Data are representative findings for three independent experimental replicates and are given as the mean ± SD. PBS, phosphate-buffered saline; LUAD, lung adenocarcinoma; NC, negative control; SAT1, spermidine/spermine N1-acetyltransferase 1; GAPDH, glyceraldehyde 3-phosphate dehydrogenase; HE, hematoxylin-eosin staining; IHC, immunohistochemical; SD, standard deviation.

cell-autonomous mechanisms of LUAD are still not fully elucidated, and further research is needed to optimize the therapeutic options available to patients. Ferroptosis is a unique form of cell death characterized by distinct mechanisms and morphological features, resulting from the accumulation of lipid peroxidation within cells in an iron-dependent manner (36-38). Studies have reported the involvement of ferroptosis in the initiation and progression of LUAD. For instance, the activation of ferroptosis by the downregulation of GINS4 inhibits LUAD progression (39), while the ferroptosis desensitized by IGF2BP3 promotes the progression of LUAD (40). Erastin was identified as a small molecule inducer of ferroptosis in 2003. It induces ferroptosis by suppressing cysteine-dependent GSH synthesis, ultimately contributing to the accumulation of ROS, MDA, and other markers of lipid peroxidation in cells (41-43). Importantly, erastin-induced ferroptotic death has been found to have significant implications in the pathogenesis of various cancer types, such as breast and liver cancer (44-46). Therefore, we leveraged the responsiveness of lung cancer cell lines to erastin treatment, specifically through the induction of ferroptosis, to better explore the regulation of ferroptosis in LUAD in this study.

Research on miRNAs in LUAD has shown that they play a critical role in the initiation, progression, and metastasis of the disease by regulating the expression of oncogenes and tumor suppressor genes. Previous studies have highlighted the diverse role of miR-9-3p in different cancer types. For example, miR-9-3p was identified as a regulator of apoptosis and proliferative activity in glioma cells (47), whereas it has been reported to inhibit carcinogenic activity in liver cancer (48). However, there have been no reports on the association between miR-9-3p and ferroptosis so far. Therefore, we innovatively studied the regulatory role of miR-9-3p in ferroptosis specifically in LUAD. Interestingly, when LUAD cells were treated with miR-9-3p inhibitor, we observed increased levels of ROS and MDA accumulation following erastin treatment, indicating an enhancement of erastin-induced ferroptosis. Moreover, while erastin treatment resulted in elevated iron levels within LUAD cells, the addition of ferrostatin-1 effectively reduced these iron levels. In contrast, treatment with either miR-9-3p mimic or inhibitor had minimal impact on the iron load in the analyzed LUAD cells. Thus, miR-9-3p is likely to influence ferroptotic activity through the regulation of lipid peroxides rather than by influencing iron accumulation. Furthermore, our research has found that the combination of miR-9-3p inhibitor and erastin treatment effectively disrupts tumor growth *in vivo* in LUAD, suggesting the potential therapeutic role of miR-9-3p inhibitors in LUAD treatment.

Further, this research suggests that SAT1, a direct target of miR-9-3p, could be mechanistically involved. Previous research has demonstrated that upregulation of SAT1 enhances lipid peroxidation and promotes ferroptotic death, ultimately suppressing tumor growth (49). Downregulation of SAT1 has also been observed in LUAD. In this study, we identified SAT1 as an important mediator of erastin-induced ferroptotic activity following the inhibition of miR-9-3p in analyzed LUAD cells. Decreased expression of SAT1 partially suppresses p53-induced ferroptosis, while the upregulation of p53 contributes to higher expression levels of SAT1 (33). Additionally, p53 is capable of inhibiting the cystine/glutamate antiporter SLC7A11 to influence ferroptotic cell death (50). In the current study, further analyses on the p53 pathway showed that in treating p53 WT LUAD cells with miR-9-3p inhibitor treatment enhanced the expression levels of both p53 and SAT1. We also observed that downregulation of SAT1 rescued these miR-9-3p inhibition-related changes in p53 and SAT1 expression. Treatment with miR-9-3p mimic blocked p53 and SAT1 expression, while the introduction of exogenous SAT1 reversed this effect and rescued p53 and SAT1 expression. Notably, in p53-mutant LUAD cells, neither the miR-9-3p inhibitors nor mimics had any effect on the expression levels of p53 and SAT1.

Conclusions

In conclusion, our study revealed that miR-9-3p exerts a negative regulatory role in ferroptosis through SAT1 and p53 signaling pathway in LUAD cells, highlight the promise of targeting miR-9-3p as a novel therapeutic approach for treating LUAD, particularly in combination with erastin to induce ferroptotic cell death. Additionally, miR-9-3p serves as promising prognostic biomarkers, providing more accurate assessments of disease progression and patient outcomes. This deepened understanding offers new avenues for improving the efficacy of LUAD treatments and optimizing clinical decision-making.

Acknowledgments

Funding: This work was supported by the "Six-One" Project for High-Level Health Talents (LGY2016037), the National Natural Science Foundation of China (82370253),

Jiangsu Provincial Research Hospital (YJXYY202204), the Innovation Team Project of Affiliated Hospital of Nantong University (XNBHCX31773), and the Postgraduate Research & Practice Innovation Program of Jiangsu Province (KYCX20-2858).

Footnote

Reporting Checklist: The authors have completed the MDAR and ARRIVE reporting checklists. Available at https://tlcr.amegroups.com/article/view/10.21037/tlcr-24-762/rc

Data Sharing Statement: Available at https://tlcr.amegroups.com/article/view/10.21037/tlcr-24-762/dss

Peer Review File: Available at https://tlcr.amegroups.com/article/view/10.21037/tlcr-24-762/prf

Conflicts of Interest: All authors have completed the ICMJE uniform disclosure form (available at https://tlcr.amegroups.com/article/view/10.21037/tlcr-24-762/coif). The authors have no conflicts of interest to declare.

Ethical Statement: The authors are accountable for all aspects of the work in ensuring that questions related to the accuracy or integrity of any part of the work are appropriately investigated and resolved. For human experiments, the study was conducted in accordance with the Declaration of Helsinki (as revised in 2013). The study was approved by the Ethics Committee of the Affiliated Hospital of Nantong University (ethical review report number: 2022-L165) and informed consent was obtained from all individual participants. For animal experiments, experiments were performed under a project license (Tab of Animal Experimental Ethical Inspection Number: S20230420-005) granted by the Laboratory Animal Center of Nantong University, in compliance with the national or institutional guidelines for the care and use of animals.

References

1. Zhang T, Wu DM, Luo PW, et al. CircNEIL3 mediates pyroptosis to influence lung adenocarcinoma radiotherapy by upregulating PIF1 through miR-1184 inhibition. Cell Death Dis 2022;13:167.
2. Travis WD. Lung Cancer Pathology: Current Concepts. Clin Chest Med 2020;41:67-85.
3. Wang Z, Zhang X, Tian X, et al. CREB stimulates GPX4 transcription to inhibit ferroptosis in lung adenocarcinoma. Oncol Rep 2021;45:88.
4. Chansky K, Detterbeck FC, Nicholson AG, et al. The IASLC Lung Cancer Staging Project: External Validation of the Revision of the TNM Stage Groupings in the Eighth Edition of the TNM Classification of Lung Cancer. J Thorac Oncol 2017;12:1109-21.
5. Chen D, Zhou H, Cai Z, et al. CircSCAP interacts with SF3A3 to inhibit the malignance of non-small cell lung cancer by activating p53 signaling. J Exp Clin Cancer Res 2022;41:120.
6. Liu S, Wang W, Ning Y, et al. Exosome-mediated miR-7-5p delivery enhances the anticancer effect of Everolimus via blocking MNK/eIF4E axis in non-small cell lung cancer. Cell Death Dis 2022;13:129.
7. Liu XS, Zhou LM, Yuan LL, et al. NPM1 Is a Prognostic Biomarker Involved in Immune Infiltration of Lung Adenocarcinoma and Associated With m6A Modification and Glycolysis. Front Immunol 2021;12:724741.
8. Sengupta D, Zeng L, Li Y, et al. NSD2 dimethylation at H3K36 promotes lung adenocarcinoma pathogenesis. Mol Cell 2021;81:4481-4492.e9.
9. Tian W, Wan X, Tian L, et al. New molecular insights into ferroptosis in lung adenocarcinoma progression and pharmacological compounds for targeted therapy. J Gene Med 2024;26:e3579.
10. Wei X, Li X, Hu S, et al. Regulation of Ferroptosis in Lung Adenocarcinoma. Int J Mol Sci 2023;24:14614.
11. Stockwell BR. Ferroptosis turns 10: Emerging mechanisms, physiological functions, and therapeutic applications. Cell 2022;185:2401-21.
12. Yang J, Mo J, Dai J, et al. Cetuximab promotes RSL3-induced ferroptosis by suppressing the Nrf2/HO-1 signalling pathway in KRAS mutant colorectal cancer. Cell Death Dis 2021;12:1079.
13. Ahola S, Rivera Mejías P, Hermans S, et al. OMA1-mediated integrated stress response protects against ferroptosis in mitochondrial cardiomyopathy. Cell Metab 2022;34:1875-1891.e7.

14. Lei G, Mao C, Yan Y, et al. Ferroptosis, radiotherapy, and combination therapeutic strategies. Protein Cell 2021;12:836-57.
15. Fang Y, Chen X, Tan Q, et al. Inhibiting Ferroptosis through Disrupting the NCOA4-FTH1 Interaction: A New Mechanism of Action. ACS Cent Sci 2021;7:980-9.
16. Gao W, Zhang T, Wu H. Emerging Pathological Engagement of Ferroptosis in Gut Diseases. Oxid Med Cell Longev 2021;2021:4246255.
17. Guo W, Wu Z, Chen J, et al. Nanoparticle delivery of miR-21-3p sensitizes melanoma to anti-PD-1 immunotherapy by promoting ferroptosis. J Immunother Cancer 2022;10:e004381.
18. Park J, Cho M, Cho J, et al. MicroRNA-101-3p Suppresses Cancer Cell Growth by Inhibiting the USP47-Induced Deubiquitination of RPL11. Cancers (Basel) 2022;14:964.
19. Wang F, Li J, Zhao Y, et al. miR-672-3p Promotes Functional Recovery in Rats with Contusive Spinal Cord Injury by Inhibiting Ferroptosis Suppressor Protein 1. Oxid Med Cell Longev 2022;2022:6041612.
20. Liu X, Gao C, Wang Y, et al. BMSC-Derived Exosomes Ameliorate LPS-Induced Acute Lung Injury by miR-384-5p-Controlled Alveolar Macrophage Autophagy. Oxid Med Cell Longev 2021;2021:9973457.
21. Zhang W, Wang L, Raza SHA, et al. MiR-33a plays an crucial role in the proliferation of bovine preadipocytes. Adipocyte 2021;10:189-200.
22. Ma LL, Liang L, Zhou D, et al. Tumor suppressor miR-424-5p abrogates ferroptosis in ovarian cancer through targeting ACSL4. Neoplasma 2021;68:165-73.
23. Zhou X, Zhuo M, Zhang Y, et al. miR-190a-5p regulates cardiomyocytes response to ferroptosis via directly targeting GLS2. Biochem Biophys Res Commun 2021;566:9-15.
24. Fan H, Ai R, Mu S, et al. MiR-19a suppresses ferroptosis of colorectal cancer cells by targeting IREB2. Bioengineered 2022;13:12021-9.
25. Wang Y, Dong L, Wan F, et al. MiR-9-3p regulates the biological functions and drug resistance of gemcitabine-treated breast cancer cells and affects tumor growth through targeting MTDH. Cell Death Dis 2021;12:861.
26. Higashi T, Hayashi H, Ishimoto T, et al. miR-9-3p plays a tumour-suppressor role by targeting TAZ (WWTR1) in hepatocellular carcinoma cells. Br J Cancer 2015;113:252-8.
27. Jiang N, Zou C, Zhu Y, et al. HIF-1α-regulated miR-1275 maintains stem cell-like phenotypes and promotes the progression of LUAD by simultaneously activating Wnt/β-catenin and Notch signaling. Theranostics 2020;10:2553-70.
28. Jing P, Xie N, Zhao N, et al. miR-24-3p/KLF8 Signaling Axis Contributes to LUAD Metastasis by Regulating EMT. J Immunol Res 2020;2020:4036047.
29. Li Z, Jiang D, Yang S. MiR-490-3p Inhibits the Malignant Progression of Lung Adenocarcinoma. Cancer Manag Res 2020;12:10975-84.
30. Wang X, Xiao H, Wu D, et al. miR-335-5p Regulates Cell Cycle and Metastasis in Lung Adenocarcinoma by Targeting CCNB2. Onco Targets Ther 2020;13:6255-63.
31. Liu M, Fan Y, Li D, et al. Ferroptosis inducer erastin sensitizes NSCLC cells to celastrol through activation of the ROS-mitochondrial fission-mitophagy axis. Mol Oncol 2021;15:2084-105.
32. Bao Z, Hua L, Ye Y, et al. MEF2C silencing downregulates NF2 and E-cadherin and enhances Erastin-induced ferroptosis in meningioma. Neuro Oncol 2021;23:2014-27.
33. Ou Y, Wang SJ, Li D, et al. Activation of SAT1 engages polyamine metabolism with p53-mediated ferroptotic responses. Proc Natl Acad Sci U S A 2016;113:E6806-12.
34. Sui X, Hu N, Zhang Z, et al. ASMTL-AS1 impedes the malignant progression of lung adenocarcinoma by regulating SAT1 to promote ferroptosis. Pathol Int 2021;71:741-51.
35. Zhang Z, Ma Y, Guo X, et al. FDX1 can Impact the Prognosis and Mediate the Metabolism of Lung Adenocarcinoma. Front Pharmacol 2021;12:749134.
36. Zhang C, Liu N. Ferroptosis, necroptosis, and pyroptosis in the occurrence and development of ovarian cancer. Front Immunol 2022;13:920059.
37. Zhou Y, Fang C, Xu H, et al. Ferroptosis in glioma treatment: Current situation, prospects and drug applications. Front Oncol 2022;12:989896.
38. Zhu J, Xiong Y, Zhang Y, et al. The Molecular Mechanisms of Regulating Oxidative Stress-Induced Ferroptosis and Therapeutic Strategy in Tumors. Oxid Med Cell Longev 2020;2020:8810785.
39. Chen L, Cai Q, Yang R, et al. GINS4 suppresses ferroptosis by antagonizing p53 acetylation with Snail. Proc Natl Acad Sci U S A 2023;120:e2219585120.
40. Xu X, Cui J, Wang H, et al. IGF2BP3 is an essential N(6)-methyladenosine biotarget for suppressing ferroptosis in lung adenocarcinoma cells. Mater Today Bio 2022;17:100503.
41. Yang Y, Sun S, Xu W, et al. Piperlongumine Inhibits Thioredoxin Reductase 1 by Targeting Selenocysteine

Residues and Sensitizes Cancer Cells to Erastin. Antioxidants (Basel) 2022;11:710.
42. Yu M, Gai C, Li Z, et al. Targeted exosome-encapsulated erastin induced ferroptosis in triple negative breast cancer cells. Cancer Sci 2019;110:3173-82.
43. Sun L, Dong H, Zhang W, et al. Lipid Peroxidation, GSH Depletion, and SLC7A11 Inhibition Are Common Causes of EMT and Ferroptosis in A549 Cells, but Different in Specific Mechanisms. DNA Cell Biol 2021;40:172-83.
44. Lee N, Carlisle AE, Peppers A, et al. xCT-Driven Expression of GPX4 Determines Sensitivity of Breast Cancer Cells to Ferroptosis Inducers. Antioxidants (Basel) 2021;10:317.
45. Li P, Lin Q, Sun S, et al. Inhibition of cannabinoid receptor type 1 sensitizes triple-negative breast cancer cells to ferroptosis via regulating fatty acid metabolism. Cell Death Dis 2022;13:808.
46. Qi W, Li Z, Xia L, et al. LncRNA GABPB1-AS1 and GABPB1 regulate oxidative stress during erastin-induced ferroptosis in HepG2 hepatocellular carcinoma cells. Sci Rep 2019;9:16185.
47. Zhen J, Zhang H, Dong H, et al. miR-9-3p inhibits glioma cell proliferation and apoptosis by directly targeting FOXG1. Oncol Lett 2020;20:2007-15.
48. Caviglia GP, Fagoonee S. Role and function of exosomal miR-9-3p in hepatocellular carcinoma. Minerva Med 2018;109:4-6.
49. Thakur VS, Aguila B, Brett-Morris A, et al. Spermidine/spermine N1-acetyltransferase 1 is a gene-specific transcriptional regulator that drives brain tumor aggressiveness. Oncogene 2019;38:6794-800.
50. Luo Y, Gao X, Zou L, et al. Bavachin Induces Ferroptosis through the STAT3/P53/SLC7A11 Axis in Osteosarcoma Cells. Oxid Med Cell Longev 2021;2021:1783485.

Cite this article as: Wu A, Zhang A, Wang T, Chen J, Shi J. Inhibition of miR-9-3p facilitates ferroptosis by activating SAT1/p53 pathway in lung adenocarcinoma. Transl Lung Cancer Res 2024;13(12):3426-3442. doi: 10.21037/tlcr-24-762